


Integrative transcriptomic profiling uncovers immune and functional responses to bisphenol a across multiple tissues in male mice

Yejee Park, Min-Jae Jang, Do-Yeal Ryu, Byeonghwi Lim, Rajesh Kumar Pathak, Myung-Geol Pang and Jun-Mo Kim 

Department of Animal Science and Technology and BET Research Institute, Chung-Ang University, Anseong, Republic of Korea

ABSTRACT

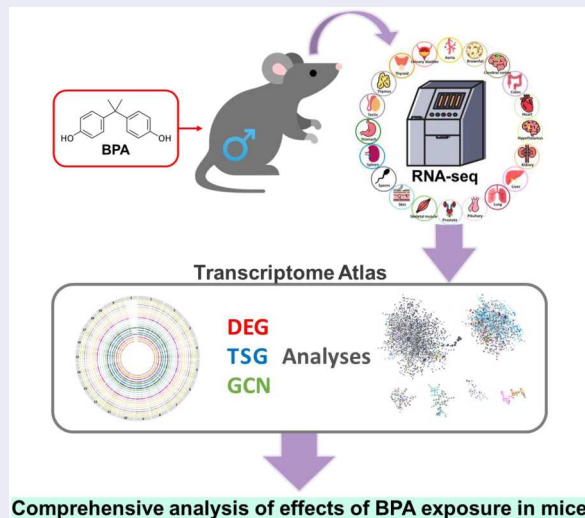
Bisphenol A (BPA), an endocrine-disrupting substance commonly found in plastics and receipts, is associated with adverse effects, including endocrine disorders, reduced fertility, and metabolic issues. To gain insights into its effects on biological systems, we observed the adverse effects of BPA in male Institute of Cancer Research (ICR) mice exposed to BPA at the lowest observed adverse effect level for 6 weeks, in comparison with the control groups. We constructed a comprehensive transcriptome profile using 20 different tissues to analyze the changes in the whole-body systems. This involved employing differential gene expression, tissue-specific gene, and gene co-expression network analyses. The study revealed that BPA exposure led to significant differences in the transcriptome in the thymus, suggesting activation of T-cell differentiation and maturation in response to BPA treatment. Furthermore, various tissues exhibited immune response activation, potentially due to the migration of immune cells from the thymus. BPA exposure also caused immune-related functional changes in the colon, liver, and kidney, as well as abnormal signaling responses in the sperm. The transcriptome analysis serves as a valuable resource for understanding the functional impact of BPA, providing profound insights into the effects of BPA exposure and emphasizing the need for further research on potential associated health risks.

ARTICLE HISTORY

Received 13 June 2024
Revised 19 August 2024
Accepted 13 October 2024

KEYWORDS




Bisphenol A (BPA); transcriptome analysis; differentially expressed gene (DEG) analysis; tissue-specific gene (TSG) analysis; gene co-expression network (GCN)




1. Introduction

Endocrine-disrupting chemicals (EDCs) negatively affect the endocrine system La Merrill et al. (2020). These substances interfere with the synthesis, secretion, transport,

binding, and elimination of hormones in the body, thereby affecting homeostasis, behavior, reproduction, and development (Ahn et al. 2022; Guarnotta et al. 2022; Ha et al. 2023). EDCs differ from hormones in

CONTACT Myung-Geol Pang  mgpang@cau.ac.kr; Jun-Mo Kim  junmokim@cau.ac.kr  Department of Animal Science and Technology and BET Research Institute, Chung-Ang University, Gyeonggi-do 17546, Anseong, Republic of Korea

 Supplemental data for this article can be accessed online at <https://doi.org/10.1080/19768354.2024.2419473>.

© 2024 The Author(s). Published by Informa UK Limited, trading as Taylor & Francis Group
This is an Open Access article distributed under the terms of the Creative Commons Attribution-NonCommercial License (<http://creativecommons.org/licenses/by-nc/4.0/>), which permits unrestricted non-commercial use, distribution, and reproduction in any medium, provided the original work is properly cited. The terms on which this article has been published allow the posting of the Accepted Manuscript in a repository by the author(s) or with their consent.

that they are not easily decomposed. Endocrine disruptors, including phthalates, polybrominated diphenyl ethers (PBDEs), and bisphenol analogs, adversely affect reproductive health Kabir et al. (2015).

Recently, given the increase in the use of disposable products, concerns regarding the effects of EDCs on human physiology have increased Pilot Program Disrupts Endocrine Disrupting Chemicals (2023). Although, EDCs are widespread in all aspects of our lives, they are not disposable Kelly et al. (2020). The EDC bisphenol A (BPA) can be exposed through normal use of packaging material, cell phone cases, receipts, and baby bottles Jalal et al. (2018). The growing interest regarding the dangers of BPA has prompted the investigation of its physiological effects Vom Saal and Vandenberg (2021). BPA is a well-known xenoestrogen that mimics the binding of estrogen to the estrogen receptor (ER) Acconcia et al. (2015). BPA induces oxidative stress to generate reactive oxygen species (ROS), which cause damage by accelerating cell dysfunction and changes in signaling pathways (Kourouma et al. 2015; Gassman 2017). BPA exposure causes adverse effects, including endocrine disorders, fertility and developmental disorders, metabolic disorders, high blood pressure, and precocious puberty Rochester (2013). Several studies have shown that animals exposed to low BPA levels have increased severity of diabetes, breast cancer, prostate cancer, decreased sperm count, reproductive problems, early maturity, and neurological problems (Melzer et al. 2012; Radwan et al. 2018). Furthermore, BPA has recently been termed an 'obesogen,' causing obesity (Vom Saal et al. 2012; Lee and Park 2019).

Because BPA is a symbolic EDC, there are many concerns regarding its effects on the reproductive system, and research has mainly focused on its effect on reproductive organs (Gurmeet et al. 2014; Matuszczak et al. 2019). To understand the molecular mechanism of BPA, next-generation sequencing (NGS) techniques, such as microarray and RNA sequencing (RNA-seq), have been used (Gao et al. 2018). A hybridization-based microarray identifies changes in gene expression patterns (Hwang et al. 2011), while RNA-seq, a cDNA sequence-based approach allows for transcriptome quantification (Jung et al. 2017; Drobná et al. 2018). However, a comprehensive analysis is required to elucidate the various mechanisms of BPA. For example, the genome atlas offers comprehensive genetic information, providing a blue print for each organ, tissue, and cell in an organism (Mure et al. 2018; Wang et al. 2019). It is especially useful to determine the physiological effects of a toxic substance such as BPA in the body from the existing state by discerning alterations in the transcriptome Wan et al. (2011). Despite the extensive research on BPA's impact on specific organs, there is still a lack

of comprehensive understanding regarding its systemic effects across multiple tissues (Costa and Cairrao 2024). Particularly, the inter-tissue interactions and the broader physiological implications of BPA exposure remain underexplored. This study aims to address this gap by providing an integrated analysis of BPA's effects across 20 distinct tissues, offering new insights into those systemic physiological effects of BPA.

This study presents a comprehensive investigation into the pervasive impact of BPA using a mouse model and a multi-faceted analytical approach. We used RNA-seq data from 20 distinct tissues to determine the effects of BPA exposure. Differentially expressed gene (DEG) analysis was conducted to determine the shift in gene expression patterns in response to BPA. Additionally, tissue specific gene (TSG) analysis enabled the pinpointing of genes that exhibited tissue-specific expression patterns under the influence of BPA. Gene co-expression network (GCN) analysis was also conducted to explore the interplay between different tissues, identifying potential correlations and mutual influences based on gene expression networks. Subsequently, the potential candidate genes were functionally annotated to understand not only the fragmented impacts of BPA on individual organs but also to comprehend the interconnected roles these organs play within the entire physiological system in response to BPA. In essence, this study provides detailed insights into EDCs, offering a holistic view of the systemic changes induced by BPA at the transcriptomic level.

2. Materials and methods

2.1. Ethical statement

All animal experiments were approved by the Institutional Animal Care and Use Committee of Chung-Ang University, Seoul, Republic of Korea (IACUC Number: 202301020018) and were conducted following the standard guidelines for animal studies.

2.2. Experimental design and sample preparation

The experimental design is illustrated in Figure 1. Eight 4-week-old CD-1 (ICR) male mice were used in this study. The mice were housed under a 12 h day/12 h night cycle at 20–25°C in an atmosphere with 50–60% humidity. Mice were allowed to adapt to the environment for one week and were separated into two groups ($n=4$ /group): control and BPA-treated. We used a BPA dose of 50 mg/kg bw/day as defined by the U.S. Environmental Protection Agency as the lowest observed adverse effect level (LOAEL) (Tyl 2009; Hengstler et al. 2011). Control mice were administered

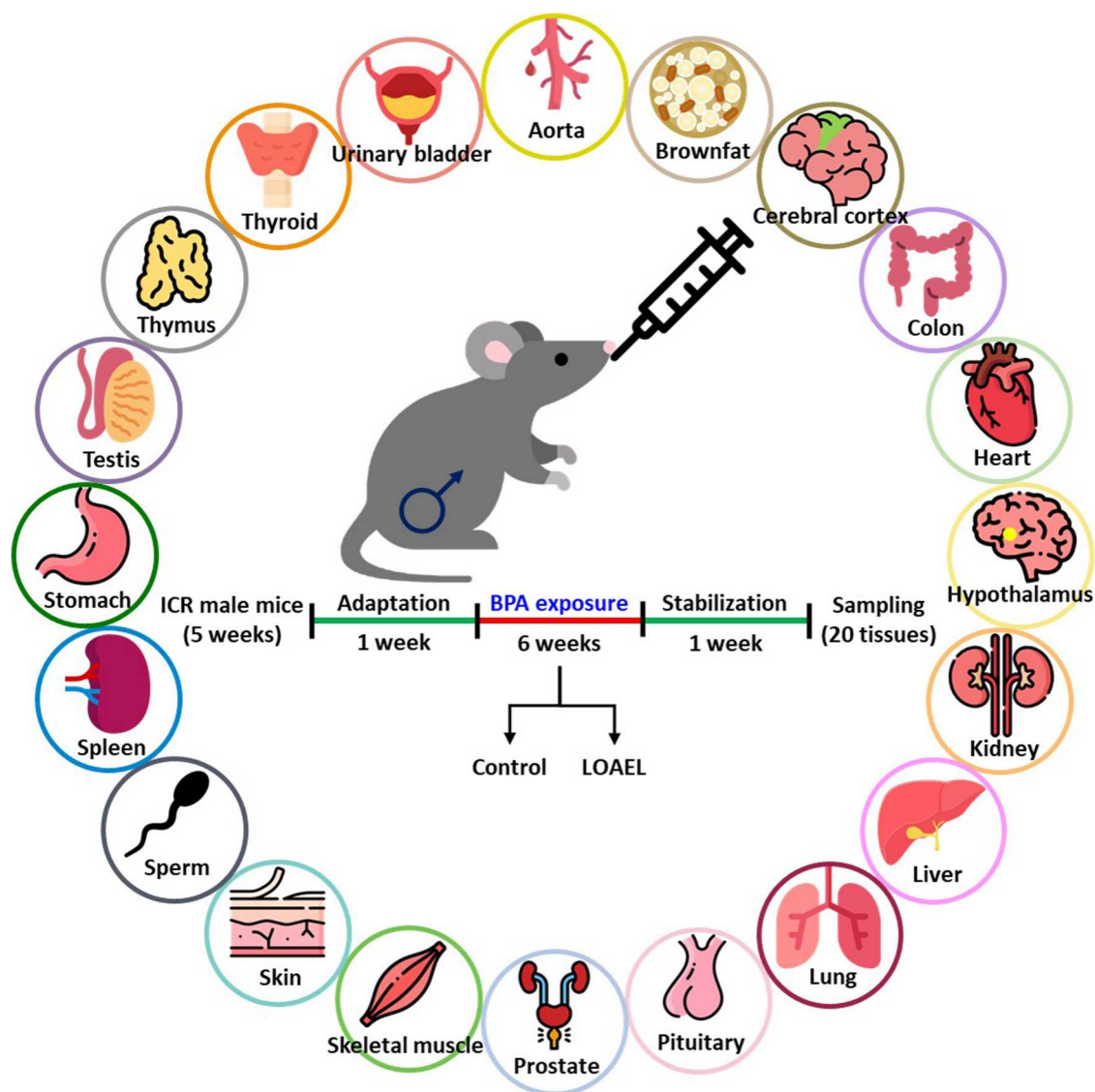


Figure 1. Experimental design of the study. A schematic diagram of the experimental design in target tissues (aorta, brown fat, cerebral cortex, colon, heart, hypothalamus, kidney, liver, lung, pituitary gland, prostate, skeletal muscle, skin, sperm, spleen, stomach, testis, thymus, thyroid, and urinary bladder) from BPA-treated mice.

vehicle (corn oil) only by oral gavage. BPA-treated were orally administered BPA according to body weight changes, following the previously mentioned dosage, for 6–11 weeks (six weeks of treatment). The mice were allowed a stabilization period of one week before sample collection. The aorta, brown fat, cerebral cortex, colon, heart, hypothalamus, kidney, liver, lungs, pituitary gland, prostate, skeletal muscle, skin, sperm, spleen, stomach, testis, thymus, thyroid, and urinary bladder were collected from each mouse. The skeletal muscle samples were collected from the hindlimb region of the mouse, and the skin samples were taken from the dorsal region after hair removal. Sperm were collected from the cauda epididymis and incubated at 37°C in 5% CO₂ for 10 min. Sperm pellets were snap-frozen in liquid nitrogen (−196°C) for RNA extraction.

Tissues other than sperm were incubated overnight at 4°C in RNAlater (Invitrogen, Carlsbad, CA, USA) and snap-frozen in liquid nitrogen (−196°C) for RNA extraction.

2.3. RNA extraction, library preparation, and sequencing

Total RNA was extracted using the QIAzol lysis reagent (Qiagen, Hilden, Germany) following the manufacturer's instructions. The total RNA concentration was calculated using Quant-IT RiboGreen (Invitrogen, Carlsbad, CA, USA). To assess the integrity of total RNA, samples were run on a TapeStation RNA ScreenTape (Agilent Technologies, Santa Clara, CA, USA). Only high-quality RNA preparations (RIN

greater than 7.0) were used for RNA library construction. A library was independently prepared with 1 µg of total RNA from each sample using the Illumina TruSeq Stranded mRNA Sample Prep Kit (Illumina, Inc., San Diego, CA, USA). First, rRNA was removed from total RNA using the Ribo-Zero rRNA Removal Kit (Human/Mouse/Rat) (Illumina, Inc., San Diego, CA, USA), and the remaining mRNA was fragmented into small pieces using divalent cations at elevated temperatures. The cleaved RNA fragments were copied into first-strand cDNA using SuperScript II reverse transcriptase (Invitrogen) and random primers. This was followed by the synthesis of second-strand cDNA using DNA Polymerase I, RNase H, and dUTP. These cDNA fragments were subjected to an end repair process, the addition of a single 'A' base, and then ligation of the adapters. The products were purified and enriched using PCR to create a final cDNA library. Libraries were quantified using the KAPA Library Quantification Kit for Illumina Sequencing platforms following the qPCR Quantification Protocol Guide (Kapa Biosystems, Wilmington, MA, USA) and qualified using a TapeStation D1000 ScreenTape (Agilent Technologies, Santa Clara, CA, USA). Indexed libraries were then submitted to an Illumina HiSeq4000 (Illumina, Inc., San Diego, CA, USA), and paired-end (2×100 bp) sequencing was performed by Macrogen, Inc. (Seoul, Republic of Korea).

2.4. NGS data processing and expression pattern analyses

The FastQC (v0.11.7) software was used to check the quality of the raw reads (Andrews 2012), and the reads were trimmed using Trimmomatic (v0.39) for low-quality reads and adapters Bolger et al. (2014). Hisat2 (v2.2.0) was used to map clean reads against the mouse reference genome (*Mus musculus*; GRCm38, GenBank assembly accession: GCA_000001635.9) of the Ensembl genome browser (http://www.ensembl.org/Mus_musculus/, accessed on July 31, 2021) using the default option of the program Kim et al. (2019). Samtools (v1.10) was used to sort the mapped reads and convert the SAM file to a BAM file Li et al. (2009). Stringtie (v2.1.4) was used for calculating the fragments per kilobase per million mapped reads (FPKM) value Pertea et al. (2015). The raw counts corresponding to the genes in each library were calculated based on exons in *Mus musculus* GTF v101 (Ensembl) as the genomic annotation reference file using featureCounts (Subread package v1.6.3) Liao et al. (2014). Expression pattern analysis was performed using the

R package 'Cluster' using the Ward's minimum variance method Struyf et al. (1997).

2.5. Differentially expressed gene (DEG) and tissue-specific gene (TSG) profiling

DEG analyses were performed by comparing the control and BPA-treated groups in each tissue and sperm samples, resulting in 20 comparisons. The R/Bioconductor edgeR package (v3.28.1) was used for DEG analyses of raw counts (Robinson et al. 2010). The trimmed mean of M-values (TMM) method was used to normalize raw counts (Robinson and Oshlack 2010). To explore the similarities among samples, we performed Multidimensional Scaling (MDS) analysis, which visualizes high-dimensional data in a lower-dimensional space, effectively illustrating the relationships between samples. This analysis was conducted using the 'limma' and 'ggplot2' R packages, which are robust tools for statistical analysis and data visualization (Wickham 2011; Ritchie et al. 2015). DEGs were identified using a negative binomial generalized linear model included in the edgeR R package Robinson et al. (2010). The cutoff for DEGs was applied using the adjusted *P*-value using the Benjamini-Hochberg correction with a false discovery rate of < 0.05 and an absolute log₂ fold change (FC) ≥ 1 (Benjamini and Hochberg 1995). For TSG profiling, a generalized linear model (GLM) was constructed using the R program based on a known method (Fang et al. 2020).

$$y = \mu + Xb + Zc + e,$$

where y is the log₂FPKM value, and μ is the intercept. X is the dummy variable for 20 tissues, where samples of the tested tissue (e.g. Aorta) are denoted as '1', whereas samples outside the same Category A (e.g. Category A) are denoted as '-1'. b is the effect of the corresponding tissue, and Z is the matrix for the covariable, which is BPA treatment. c is the corresponding covariable effect, and e is the residual effect.

To categorize tissue-specific genes, a generalized linear model (GLM) was utilized through three distinct models, each addressing a specific aspect of gene expression related to BPA treatment. Model 1 aimed to identify genes with tissue-specific expression patterns without considering the influence of BPA treatment. This initial model focused solely on capturing genes that exhibit distinct expression profiles in different tissues. Model 2 expanded upon Model 1 by incorporating BPA treatment as a covariable. The purpose of this model was to discern tissue-specific genes that show significant changes in expression due to BPA exposure, highlighting how BPA treatment affects gene expression

within specific tissues. Model 3 further refined the analysis by applying additional thresholds to both the BPA treatment covariable and the significance level. This model aimed to identify tissue-specific genes that exhibit statistically significant changes in expression in response to BPA, providing a more stringent assessment of BPA's impact.

2.6. Gene co-expression network (GCN) analysis

GCN analysis was conducted using two methods. First, the partial correlation and information theory (PCIT) algorithm was used to perform GCN analysis Watson-Haigh et al. (2010). Using the first GLM result, we constructed the network with the genes of absolute co-expression correlations of ≥ 0.95 . The most significant genes (third GLM result) were included.

We also performed weighted gene co-expression network analysis (WGCNA) using the second GLM result (Zhang and Horvath 2005). Twenty tissues were used as traits, and the Pearson method was used to evaluate the correlation. The soft threshold (power) was chosen using the 'pickSoftThreshold' function in the WGCNA R package, and the hard threshold using 0.1 in each module was used for filtering (Langfelder and Horvath 2008). Afterward, the network was reconstructed using the 'aracne' function in bnlearn R package (Zheng and Huang 2018).

Results of GCN analyses were visualized using Cytoscape (v3.7.2) software and comprised genes (nodes) included in the network and the connections (edges) between genes. The maximum value of expression among tissues is presented as the color of each node.

2.7. Functional analyses of DEGs and GCNs

The functions of DEGs and GCN nodes were annotated using Database for Annotation, Visualization and Integrated Discovery (DAVID; <https://david.ncifcrf.gov/>) v6.8 (Dennis et al. 2003). Gene ontology (GO) terms and Kyoto Encyclopedia of Genes and Genomes (KEGG) pathways were used for functional analyses of the DEGs corresponding to 20 tissues and two types of GCNs. In the GO terms, biological processes (BP), cellular components (CC), and molecular functions (MF) were included. GO-BPs were visualized using tables and dotted plots. The treemap constructed using REVIGO (<http://revigo.irb.hr/>) was used to present GO terms with default advanced options Supek et al. (2011). KEGG annotations were enriched based on $-\log_{10}P$ -value and fold enrichment and shown in the bar graph. All data used in the enrichment analyses were annotated for *Mus musculus*.

3. Results

3.1. Overview of RNA-Seq data processing and DEG analysis

In this study, we used 20 tissue samples (aorta, brown fat, colon, cerebral cortex, heart, hypothalamus, kidney, liver, lung, pituitary gland, prostate, skeletal muscle, skin, sperm, spleen, stomach, testis, thymus, thyroid, and urinary bladder) from eight individuals (four control groups and four BPA-treated groups). Four billion paired-end sequence reads were generated from 161 tissue samples, with an average of 24.9 million reads per sample. The clean reads that passed the trimming process averaged 24.1 million, with an average trimming rate of 3.48%. Trimmed reads were mapped with an average unique mapping rate of 82.18% and an average overall mapping rate of 94.84% to mouse reference genome GRCm38 (Table S1). The transcriptome after BPA treatment showed clear separation for each tissue type in the MDS plot (Figure 2). Expression pattern analysis of 161 samples was performed, and most samples were clustered by tissue; tissues showing similar expression patterns were grouped (category A: aorta, brown fat, heart, and skeletal muscle; category B: cerebral cortex and hypothalamus; category C: colon, kidney, lung, pituitary gland, prostate, skin, stomach, thyroid, urinary bladder; category D: liver; category E: spleen and thymus; category F: sperm; category G: testis), as shown in Figure S1. A Circos plot was generated to display the BPA-treated transcriptome at the location of the corresponding chromosome. Each dot represents the transcriptome, indicating the starting position on the chromosome, and the expression level was normalized to the z-score of logFPKM values, which were derived from normalized expression values of FPKM. The Circos plot includes DEGs, which were confirmed by comparing the gene expression level of the BPA-treated group with that of the control group (up-regulated DEG: red, down-regulated DEG: blue). A total of 37,077 genes were tested in the DEG analyses. The number of tested genes varied depending on the expressed genes in each tissue: aorta = 16,129; brown fat = 15,360; colon = 17,963; cerebral cortex = 17,999; heart = 14,674; hypothalamus = 18,940; kidney = 17,206; liver = 14,504; lung = 18,609; pituitary gland = 17,047; prostate = 18,346; skeletal muscle = 14,880; skin = 18,729; sperm = 29,661; spleen = 18,463; stomach = 17,698; testis = 22,873; thymus = 17,993; thyroid = 18,693; and urinary bladder = 18,668. The expression levels in the sperm and testis were relatively high for every chromosome, particularly chromosome Y (Figure 2). The numbers of DEGs in the

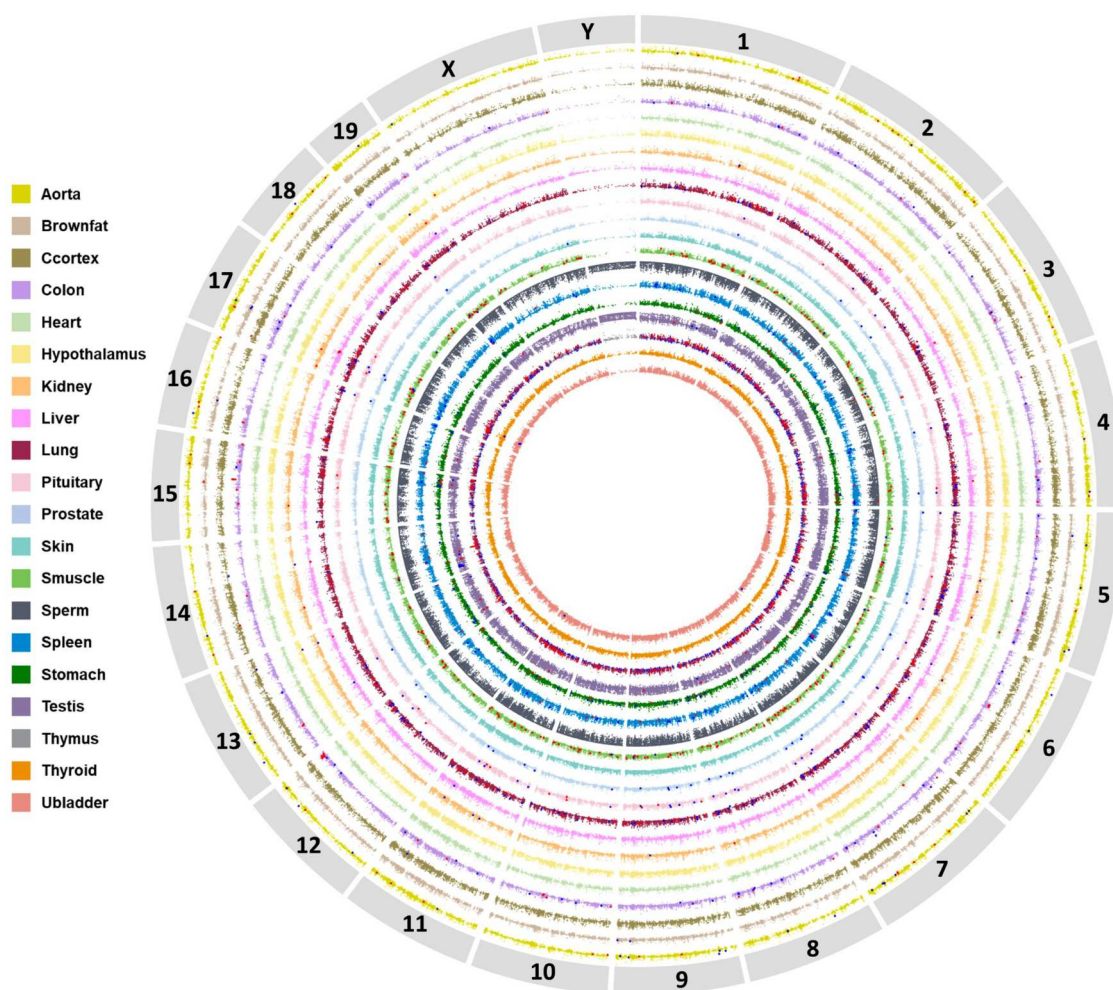


Figure 2. Overview of the transcriptome expression of 20 tissues affected by BPA. Circos plot showing the transcriptome patterns according to chromosome location (border). The 20 tissues are indicated in legend by the colors on the left side of the Circos plot. Up-regulated and down-regulated differentially expressed genes (DEGs) are indicated by red and blue dots, respectively. Circos plot features a central multidimensional scaling (MDS) plot depicting the clustered distribution of 161 samples.

20 tissues are shown in Table S2. The thymus had the largest number of DEGs ($n = 8,579$), including 4,455 up-regulated DEGs and 4,124 down-regulated DEGs. The lungs ($n = 372$), skeletal muscle ($n = 315$), colon ($n = 115$), spleen ($n = 100$), and aorta ($n = 80$) followed, in that order. DEG analysis revealed that the number of DEGs was small in several tissues, and it was difficult to perform subsequent functional analyses for these tissues.

3.2. Functional annotations of DEGs

To investigate BPs related to BPA treatment, functional enrichment analyses of the DEGs based on the GO and KEGG databases were performed. As shown in the BP treemap of the total DEGs in the thymus, the most DEG-rich tissue, positive regulation of cell migration was identified as the representative term (Figure 3a). Specifically, immune-related pathways (systemic lupus

erythematosus, Th1 and Th2 cell differentiation, and Th17 cell differentiation) were the main KEGG pathways in the up-regulated results, and cell metabolism and signaling-related pathways (metabolic pathways, PI3K-Akt signaling pathway, rap1 signaling pathway, and calcium signaling pathway) were the representative KEGG pathways among down-regulated results (Figure 3b, c). The next most DEG-rich tissues were the aorta, colon, lungs, skeletal muscle, and spleen. Similar to the thymus, immune-related BP terms (response to bacterium, inflammatory response, regulation of immune response, immune system process, and immune response) were up-regulated, except in the aorta, and protein folding-related BP terms (response to unfolded protein, chaperone-mediated protein folding requiring cofactor, protein refolding, protein folding, and cellular response to unfolded protein) were down-regulated, excluding the skeletal muscle (Figure S2).

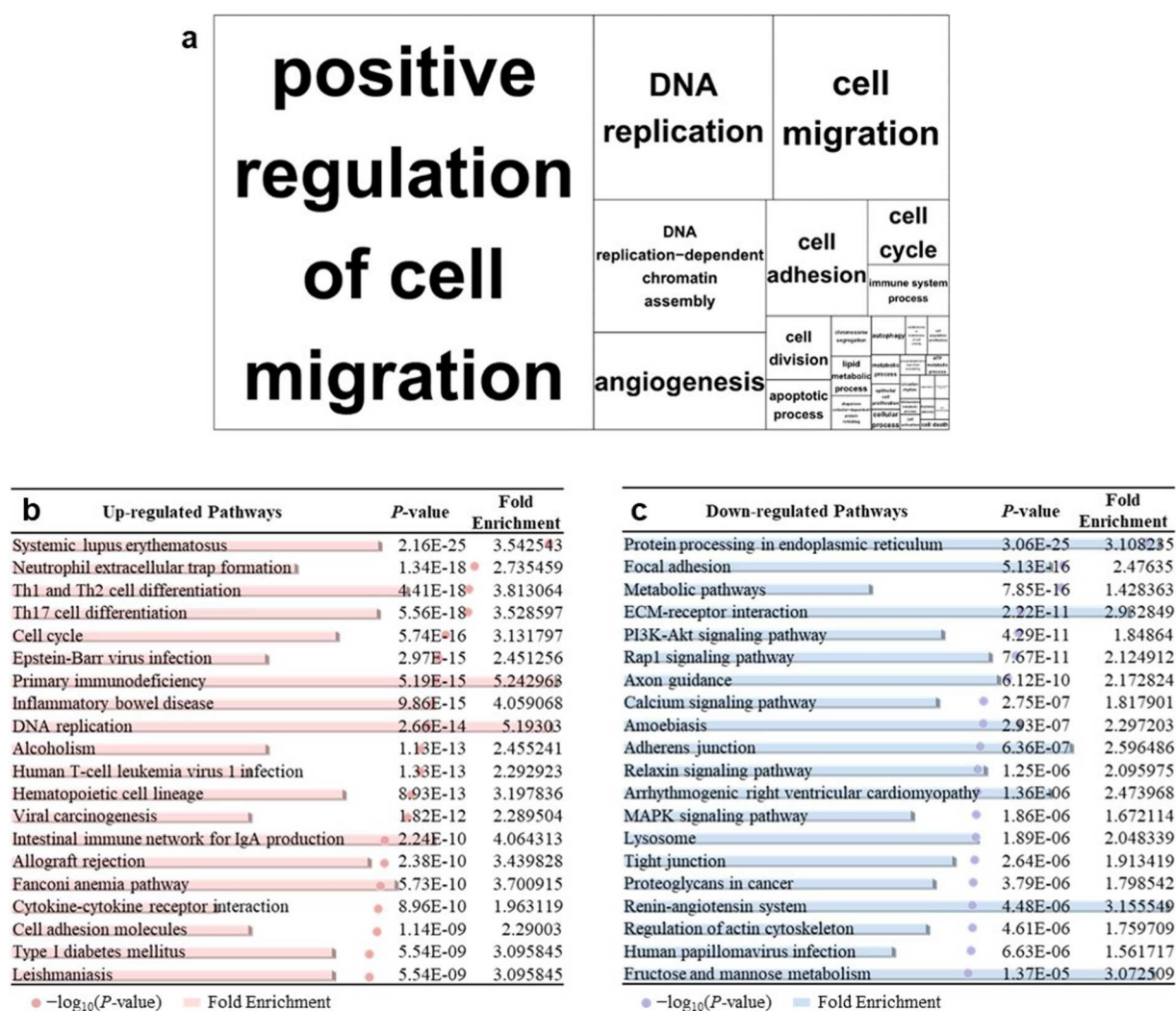


Figure 3. Functional analysis for DEGs in thymus exposed to BPA. (a) Treemap of the biological process. (b-c) The 20 most significant KEGG pathways associated with up-regulated/down-regulated DEGs. $-\log_{10}(P\text{-value})$ and fold enrichment are shown at the background of the table as explained.

However, in the case of tissues with very few DEGs (cerebral cortex, heart, hypothalamus, skin, sperm, and thyroid), functional analysis could not be performed. Despite functional annotation, the tissues that showed relatively few results were brown fat, kidney, liver, pituitary gland, prostate, and urinary bladder. In brown fat and the urinary bladder, only two genes (*H2-EBI* and *GM1127*) were involved in the functional results and were down-regulated. The most significant KEGG pathways were graft-versus-host disease and allograft rejection. Antigen processing and presentation were the most notable GO terms. Similarly, in the kidney, every functional result was down-regulated, and the largest proportion of BP terms were immune-related (cellular response to interferon-beta, defense response, defense response to protozoan, and immune response). In contrast, the liver showed only up-regulated expression

with the same pathways as those in brown fat and urinary bladder, including expression of *H2-T10* and *H2-BL*. The pituitary gland and prostate tissues identified protein processing in the endoplasmic reticulum as the most significant KEGG pathway and protein folding-related terms (protein folding, unfolded protein binding, and protein refolding) were down-regulated and considered significant GO terms.

3.3. TSG analysis

Through GLM with different cut-offs, three types of tissue-specific gene sets were identified (Table S3). Model 1 did not include the effect of BPA treatment, and only the top 1% of the GLM results for each tissue was used. The total number of TSGs calculated using Model 1 was 7,244, including 3,683 and 3,561 highly

expressed genes in the control and BPA-treated groups, respectively. Model 2 included the effect of BPA as Z (covariable), and the significance level of b (corresponding tissue effect) was limited to P -value < 0.05 . As a result of GLM model 2, 2,839 genes were selected as TSGs in 20

tissues, including 1,674 genes that were highly expressed in the control group and 1,165 genes that were highly expressed in the BPA-treated group. Model 3 was Model 2 with an additional threshold of Z (covariable) and a P -value < 0.05 . GLM Model 3 resulted

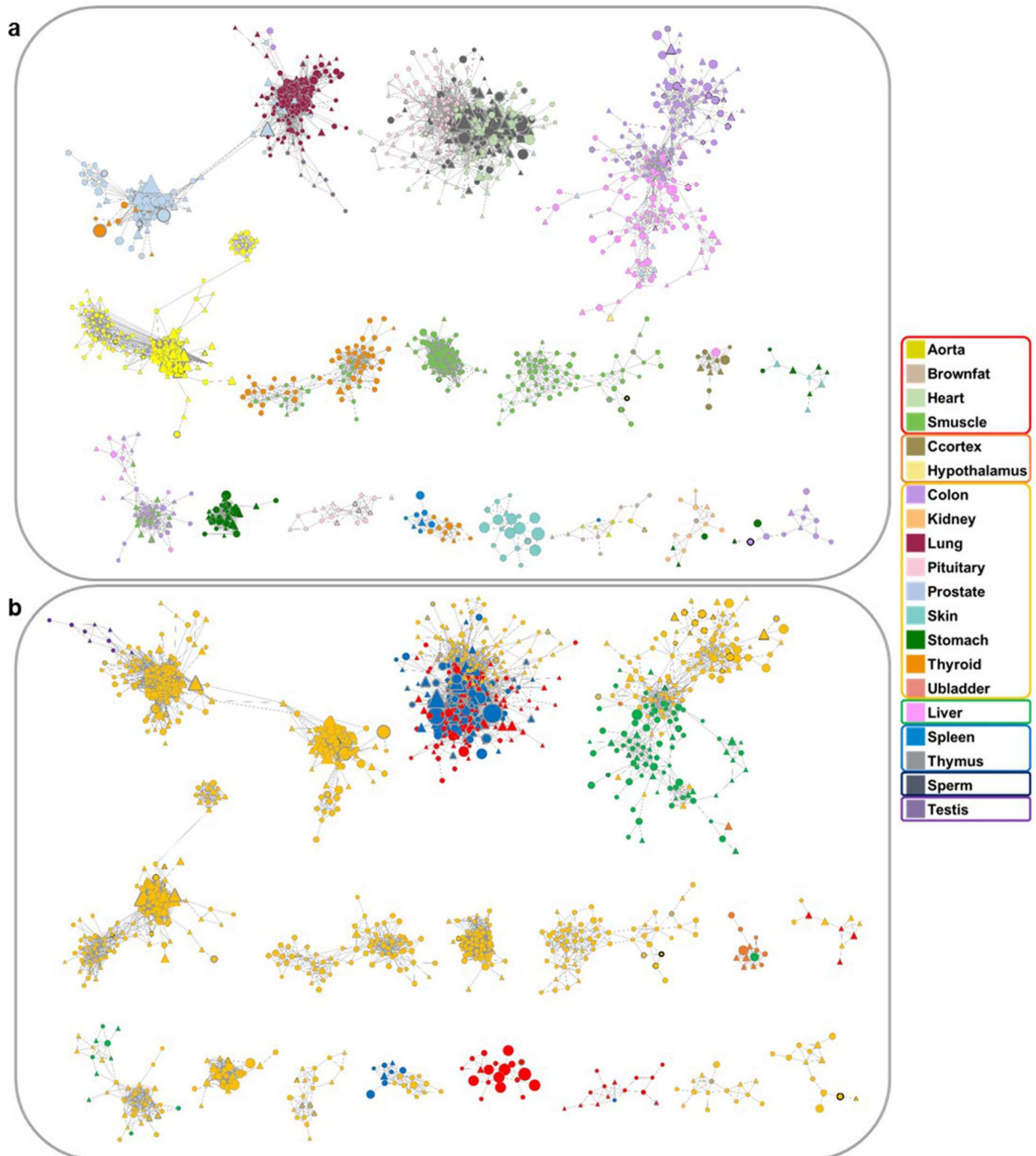


Figure 4. PCIT networks. (a) PCIT networks of 20 tissues. (b) Network for the seven categories (category A: aorta, brown fat, heart, and skeletal muscle; category B: cerebral cortex and hypothalamus; category C: colon, kidney, lung, pituitary gland, prostate, skin, stomach, thyroid, urinary bladder; category D: liver; category E: spleen and thymus; category F: sperm; category G: testis). Node color indicates the tissue (20 colored squares) or category (7 border colors) in the legend. The node border indicates the TSG of model 3, and the size of the node indicates the expression. The shape of the node indicates genes expressed in the control (ellipse) and treatment (triangle) groups.

in 966 TSGs with 506 and 460 genes expressed in control and treatment groups.

3.4. GCN analysis and functional annotations for PCIT results

The gene co-expression network obtained using the PCIT algorithm comprised 1,485 nodes and 31,250 edges (Figure 4a). The color of the nodes indicates the

tissue representing the maximum average expression level in the TSG among 20 tissues. The border of the node shows TSGs of Model 3 in the network, and the expression level of the gene is shown as the node size. The shape of the node indicates whether it is a control-expressed gene (eclipse) or a treatment-expressed gene (triangle). Classifying the same network into seven categories revealed that several genes in category C constituted the network (Figure

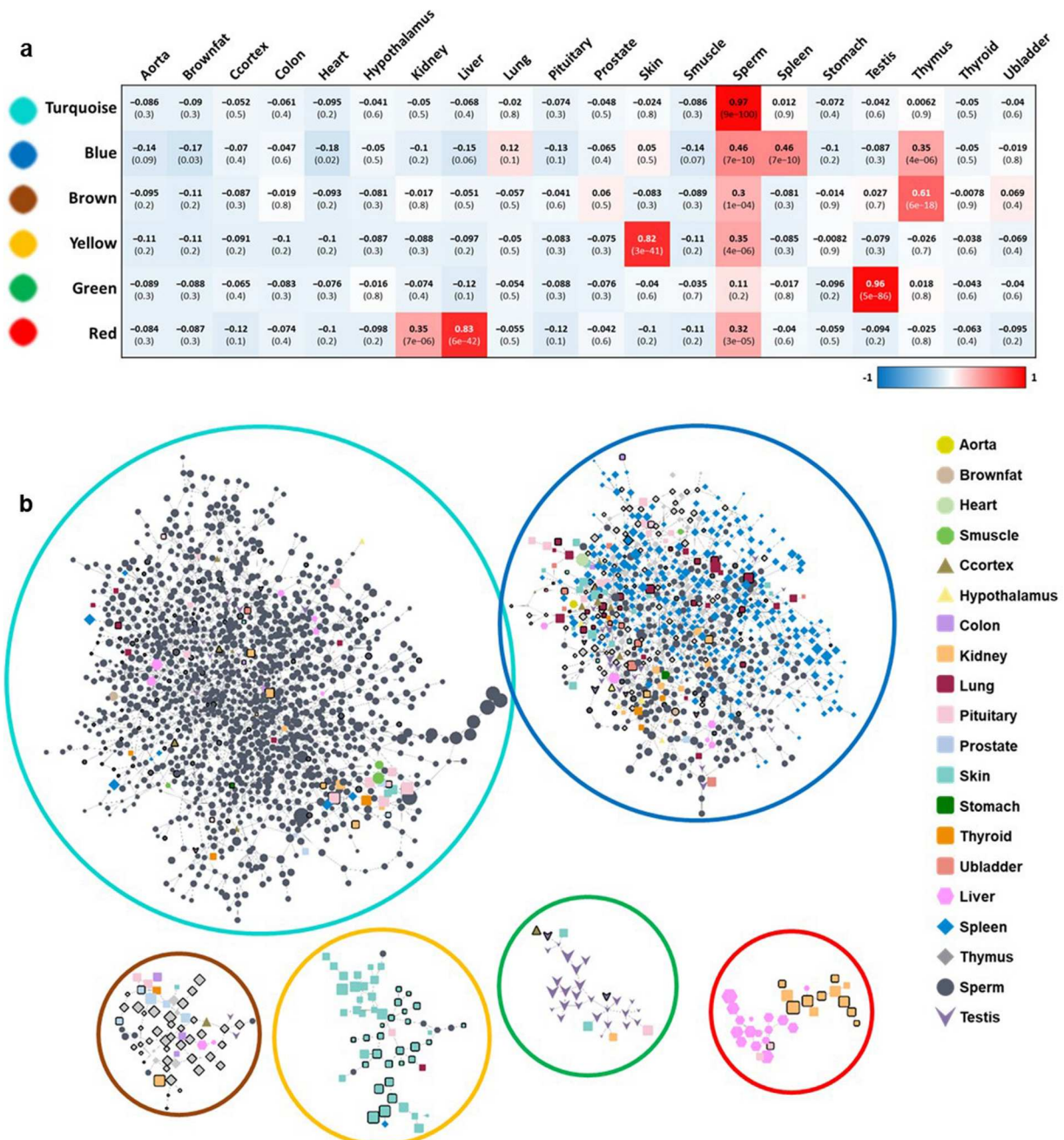


Figure 5. Weighted gene co-expression network analysis (WGCNA). (a) Module-trait correlation heatmap. Correlation of 6 modules and 20 tissues calculated by WGCNA. (b) Gene co-expression network constructed using WGCNA. Node colors indicate 20 different tissues, and the border of the node indicates 7 categories (category A: octagon; category B: triangle; category C: round rectangle; category D: hexagon; category E: diamond; category F: ellipse; category G: V shape).

4b). The corresponding network was divided into 17 subnetworks (SNs) (Fig. S3). Information on the SN is presented in Table S4, along with the number of nodes and edges. The largest of the 17 SNs was SN1, which mostly comprised the lung and prostate and included five tissues (colon, lung, prostate, testis, and thyroid). Four SNs comprised three different tissues: SN2, SN3, SN10, and SN15. SNs composed of two tissues accounted for the most number at seven, followed by SNs composed of only one tissue at five. SN1, SN3, SN4, SN6, SN7, SN11, SN12, and SN17 were included in the TSG results of Model 3, and SN3 and SN4 were significantly associated with BPA treatment. SN3 mostly comprised the colon and liver, and the BP terms included immune-related terms (adaptive immune response, positive regulation of T cell proliferation, and immune system process). In addition, the KEGG pathway displayed similar immune-related pathways (primary immunodeficiency, T-cell receptor signaling pathway, B-cell receptor signaling pathway, intestinal immune network for IgA production, natural killer cell-mediated cytotoxicity, and cytokine-cytokine receptor interaction) as BP terms (Fig. S4a, b). SN4, which consists of the kidney and skin TSG, had blood coagulation as the largest BP term. Similarly, the complement and coagulation cascades were the most remarkable KEGG pathway, followed by metabolic pathways and steroid hormone biosynthesis (Fig. S4c, d).

3.5. GCN analysis and functional annotations for WGCNA results

To identify different co-expressed modules after BPA treatment in 20 tissues, WGCNA was conducted based on the pairwise correlation of gene expression for the 2,839 genes in GLM model 2. The number of genes in the modules ranged from 30 to 1,300 (Table S5), and the correlation matrix between the modules and 20 tissues was visualized using a heatmap (Figure 5a). A whole-gene co-expression network using WGCNA, composed of six modules, resulted in 2,275 nodes and 2,875 edges (Figure 5b). The turquoise module, which was positively correlated with a coefficient of 0.97 in sperm, was the largest with 1,300 nodes and 1,626 edges. The most representative BP term was the G protein-coupled receptor signaling pathway (Figure 6a), which consists of subordinate terms related to responses to stimuli, such as the sensory perception of smell, detection of chemical stimuli involved in the sensory perception of smell, and detection of temperature stimuli involved in the sensory perception of pain. The immune response, cellular response to interferon-beta, and regulation of type interferon production

were sub-terms of immunoglobulin production (Table 1). The blue module showed a positive correlation with the sperm (0.46), spleen (0.46), and thymus (0.35). The largest contributing BP term was the cell surface receptor signaling pathway, comprising immune-related receptor signaling pathways (Figure 6b, Table 1). Similarly, the KEGG pathway analysis revealed cytokine- and chemokine-related pathways, such as viral protein interaction with cytokine and cytokine receptor (Figure S5a). The brown module showed a positive correlation (0.61) with the thymus, displaying the regulation of systemic arterial blood pressure and zymogen activation as representative BP terms (Figure 6c, Table 1). Among the enriched KEGG pathways, the renin-angiotensin system was significant, and other enriched signaling pathways are presented in Figure S5b. The yellow module with the highest correlation with the skin exhibited the regulation of cytokine production as a significant BP term

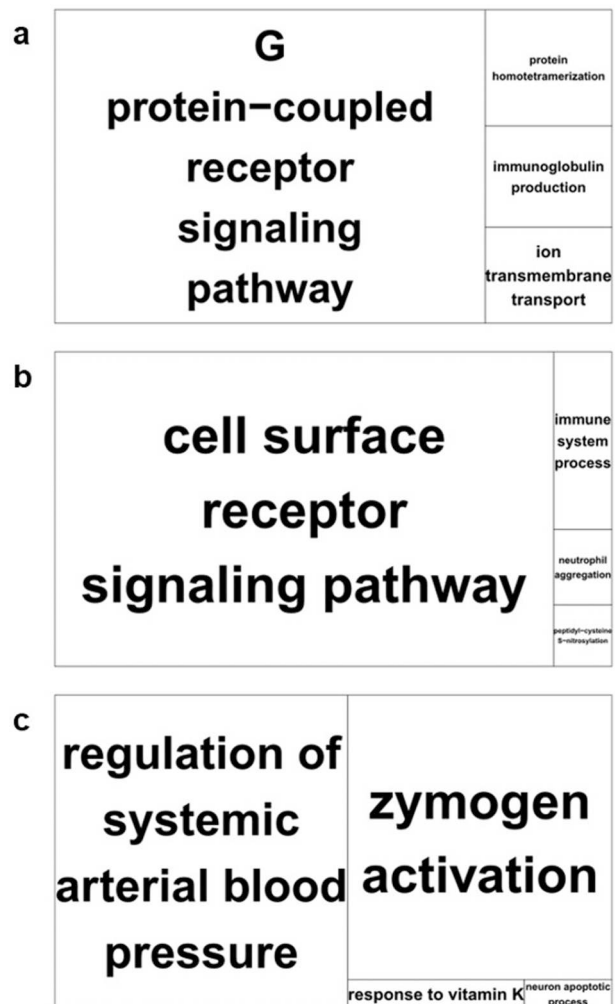


Figure 6. Functional analysis results (BP terms) for turquoise, blue, and brown modules. (a) BP treemap of the turquoise module. (b) BP treemap of the blue module. (c) BP treemap of the brown module.

Table 1. Subordinate biological process (BP) terms related to WGCNA modules.

WGCNA module	BP term	P-value	Fold Enrichment
Turquoise module	G protein-coupled receptor signaling pathway		
	sensory perception of smell	2.37E-09	3.71499
	G-protein coupled receptor signaling pathway	5.84E-06	2.54475
	response to stimulus	1.44E-04	5.89845
	detection of chemical stimulus involved in sensory perception of smell	1.55E-03	17.27129
	detection of temperature stimulus involved in sensory perception of pain	7.96E-03	22.02090
	detection of chemical stimulus involved in sensory perception of pain	2.01E-02	97.87065
	visual perception	2.02E-02	4.79758
	detection of chemical stimulus involved in sensory perception of pain	6.56E-02	29.36119
	immunoglobulin production		
	immune response	1.42E-03	3.41409
	cellular response to interferon-beta	7.81E-03	9.78706
	regulation of type I interferon production	3.99E-02	48.93532
	immunoglobulin production	7.92E-02	3.96773
Blue module	cell surface receptor signaling pathway		
	cell surface receptor signaling pathway	3.58E-13	11.38353
	immunoglobulin production	1.83E-08	10.56309
	immune response	2.25E-08	5.23316
	neutrophil chemotaxis	2.60E-06	13.02781
	inflammatory response	6.96E-06	4.81239
	positive regulation of GTPase activity	1.26E-05	5.46622
	lymphocyte chemotaxis	8.71E-05	21.01260
	monocyte chemotaxis	1.76E-04	17.60515
	positive regulation of T cell proliferation	2.54E-04	10.56309
	cellular response to interleukin-1	3.88E-04	9.65023
	eosinophil chemotaxis	5.23E-04	24.81488
	chemokine-mediated signaling pathway	5.27E-04	13.29369
	positive regulation of interferon-gamma production	5.39E-04	8.98470
	T cell costimulation	8.84E-04	20.84450
	cellular response to interferon-gamma	1.49E-03	7.17127
	negative thymic T cell selection	4.95E-03	27.91675
	T cell receptor signaling pathway	6.98E-03	6.57970
	positive regulation of immunological synapse formation	1.52E-02	130.27815
	chemotaxis	1.94E-02	4.86112
	positive regulation of neutrophil chemotaxis	2.05E-02	13.47705
	cell chemotaxis	2.72E-02	6.13074
	positive regulation of natural killer cell mediated cytotoxicity	2.76E-02	11.49513
	T cell homeostasis	2.76E-02	11.49513
	natural killer cell mediated immunity	3.02E-02	65.13907
	positive regulation of ERK1 and ERK2 cascade	3.48E-02	3.31216
	negative regulation of leukocyte tethering or rolling	3.76E-02	52.11126
positive regulation of natural killer cell degranulation	4.49E-02	43.42605	
positive regulation of interleukin-12 production	4.62E-02	8.68521	
positive regulation of B cell proliferation	4.81E-02	8.49640	

(Figure S6). Finally, the liver- and kidney-related red modules showed the largest proportion of BP terms related to response to chromate (Figure S7).

4. Discussion

In this study, we investigated the complex correlation induced by BPA exposure in various mouse tissues to elucidate its potential implications for human health. BPA, a ubiquitous compound present in everyday items such as water bottles, food containers, and receipts, induces toxicity and various disorders (Abraham and Chakraborty 2020; Manzoor et al. 2022). Its pervasive concentrations across various environments and products have raised considerable concerns about its several adverse effects (Vom Saal and Vandenberg 2021). BPA has drawn significant attention due to its anti-androgenic and estrogen-mimicking effects, which confirm its role as an endocrine

disruptor and its potential impact on human reproduction Ma et al. (2019). Notably, BPA can negatively affect the neuroendocrine process, particularly the regulatory mechanisms of the hypothalamus–pituitary–gonadal axis Xi et al. (2011). Given that hormonal fluctuations in female mice could introduce variability into the experimental outcomes, male mice were selected for this study to minimize such influences and to more clearly assess the direct impact of BPA. Disruption of the hypothalamic–pituitary–testicular (HPT) axis can lead to decreased sperm quality Wisniewski et al. (2015). Additionally, BPA induces oxidative stress, reducing sperm motility and causing oxidative damage in the brain and testes Sadek et al. (2014). Studies have also shown that BPA causes obesity (Vom Saal et al. 2012; Acconcia et al. 2015). In summary, BPA may have multiple effects on the whole-body system as well as the reproductive system.

Thorough transcriptome profiling enables comprehensive studies that go beyond the scope of fragmentary transcriptome analyses, which typically focus on specific genes or proteins (Norreen-Thorsen et al. 2022; Abbassi-Daloi et al. 2023). By analyzing the transcriptomes of entire genomes using various approaches, researchers can gain insights into gene expression patterns, including gene expression levels and locations (Kukurba and Montgomery 2015; Abbassi-Daloi et al. 2023). This approach can uncover genes that play crucial roles in the initiation and progression of diseases, which not only clarifies associated biological processes but also enhances the understanding of disease etiology and elucidation of the underlying mechanisms (Yin et al. 2014; Sukjamnong et al. 2020; Kim et al. 2021; Satam et al. 2023). Therefore, in-depth transcriptome studies are vital tools for analyzing genes related to diseases and biological changes. This comprehensive approach paves the way for a deeper understanding of the complex interplay of genes within biological systems. Through an intricate RNA-seq analysis spanning 20 distinct mouse tissues exposed to BPA, our investigation was able to narrow down into three complex interactions caused by BPA.

4.1. Regulation of sperm function and reproductive health

WGCNA provides a comprehensive view of the modules co-expressed across TSGs and related tissues, revealing key biological functions and hub genes (Figure 5b). This simplifies the interpretation of various gene responses in several co-expression modules Niemira et al. (2019). Among the six modules, the turquoise module displays the G protein-coupled receptor (GPCR) signaling pathway and the *OLFR* gene as the primary term and novel gene, respectively.

GPCRs are a family of cell surface receptors that bind extracellular molecules and activate intracellular responses (Weis and Kobilka 2018). The *OLFR* genes encode GPCRs. GPR30, a type of GPCR, uniquely responds to sex hormones such as estrogen. It binds the sperm cell membrane and is renamed as the G protein-coupled estrogen receptor (GPER) (Chevalier et al. 2012; Adegoke et al. 2020). GPCRs, including *ADRA2A*, *AGTR1*, *AGTR2*, *FZD3*, and *GLP1R*, are involved in specific sperm functions, such as capacitation, acrosome reaction, and motility Corda et al. (2022). The acrosome reaction is triggered by an increase in cytosolic calcium concentration (Ca^{2+}) within sperm, mediated by GPER activation Gao et al. (2022).

Previous studies have shown that BPA, which mimics the function of estrogen receptors, can negatively affect

spermatogenesis. Wisniewski et al. showed that estrogen receptor alpha operates in the early stages of the HPT axis, regulating several signaling pathways involved in spermatogenesis in the testis Wisniewski et al. (2015). Castellini et al. found that BPA exposure in men was associated with reduced sperm counts and motility Castellini et al. (2020). Further, González-Rojo et al. revealed that BPA exposure in zebrafish led to impaired spermatogenesis and induced histone hyperacetylation in the testes González-Rojo et al. (2019). A comprehensive review of the molecular mechanisms underlying BPA action in spermatozoa by Rahman and Pang concluded that BPA can disrupt spermatogenesis at various stages (Rahman and Pang 2019). Krzastek et al. highlighted BPA as a major concern when discussing the impact of environmental toxin exposure on male fertility potential (Krzastek et al. 2020). These findings collectively suggest that BPA negatively affects male fertility, particularly spermatogenesis.

Our network analysis results contribute to a deeper understanding of the toxicological effects of BPA. They also aid in the development of strategies to mitigate its impact on male fertility. Further research in these areas could provide valuable insights into the molecular mechanisms of action of BPA in spermatozoa and its potential effects on male fertility.

4.2. Heat shock proteins (HSPs): key players in protein folding and cellular stress responses

Our DEG annotation revealed that among the down-regulated DEGs, those encoding proteins crucial for protein folding-related functions were predominant (Figure S2). This observation is consistent with previous research findings linking BPA to alterations in protein folding, modification, and metabolism (Chen et al. 2015).

Heat shock proteins (HSPs) are crucial in various physiological processes, including protein folding-related mechanisms Hu et al. (2022). They are expressed in cells exposed to stress factors such as heat, chemicals, or radiation Park et al. (2023). HSPs help to stabilize protein structure, prevent misfolding, and maintain the stability of properly folded proteins Lang et al. (2021). HSP90 is the most important for protein folding. HSP90 binds to a variety of proteins to stabilize their structure. It is particularly important for the folding of proteins involved in cell signaling, cell division, and cell death (Xu et al. 2012; Ren et al. 2022). It has also been associated with colorectal cancer (Papaconstantinou et al. 2001; Hackl et al. 2010).

This interplay of BPA on protein folding and immune function suggests its role in inducing cellular stress, potentially compromising cell survival and function. It

suggests a potential negative effect of BPA on the immune system.

4.3. BPA exposure induces widespread immune-related responses across diverse tissues

Up-regulated DEGs from various tissues, including the thymus, brown fat, colon, heart, kidney, liver, lung, skeletal muscle, stomach, and urinary bladder, suggested an immune-related response as the primary biological effect of BPA treatment. The thymus, a primary immune organ, exhibited an enhanced immune-related response (Figure 3b). As the thymus is composed of T lymphocytes derived from bone marrow progenitor cells and serves as the site for T lymphocyte maturation, it exhibits prominent helper T cell differentiation and hematopoietic cell lineage Aydemir et al. (2018). BPA induces an inflammatory response through various cell signaling pathways, aligning with the overlapping KEGG pathway results for up-regulated DEGs (Murata and Kang 2018).

GCN analysis suggested the involvement of enriched pathways, highlighting altered tissue-specific effects of BPA exposure (Figure 4). Notably, subnetworks SN3 and SN4 from the PCIT algorithm were particularly significant (Figure S3). SN3, comprising the colon, hypothalamus, liver, and prostate tissues, echoed the involvement of immune-related pathways observed in the DEG results. TSGs such as *RAG2* and *CD27* underpin their potential impact on T cell development and maintenance (Collins et al. 1996; Hendriks et al. 2000). T cell receptor genes such as *TRBV* and *TRAJ* recognize antigenic peptides and bind to major histocompatibility complex (MHC) molecules, which are complex heterodimers Massari et al. (2018). Our results suggest that the colon and liver significantly influence the binding of T cells to their receptors.

SN4, composed of kidney and skin tissues, revealed blood coagulation as a notable term, with serine-protease inhibitor (*SERPIN*) genes being the most significant. *SERPIN* genes are circulatory protein-coding genes that play roles in coagulation, inflammation, and immune response El-Hefnawy et al. (2022). These genes are associated with chronic kidney diseases and immunological Th1 responses Sánchez-Navarro et al. (2021). Therefore, BPA-exposed mice show alterations in several biological processes related to immune cell development and T cell immunity generation in the colon and liver, and BPA can cause serious damage to the kidney.

The blue module from the WGCNA is associated with cell-surface receptor signaling pathways, offering insights into immune-related binding reactions, such

as T cells and cytokine receptors. The major genes related to the corresponding terms were *CD3*, which is related to T cell receptor expression, and *CD40*, which participates in the mediation of immune and inflammatory responses. Our results suggest that the spleen exhibits immune-related under the effect of BPA, which is in line with a previous study that showed that BPA caused an increase in the immunoreactivities of *CD3*, *CD4*, and *CD8* in lymphocytes and *IL-4* and *IFN-γ* levels in the spleen Yoshino et al. (2004).

The brown module from the WGCNA is associated with zymogen activation and the renin-angiotensin system, which regulates physiological functions in response to stimuli. The renin-angiotensin system, the most enriched KEGG pathway, involves kallikrein 1 (*KLK1*) genes that are implicated in carcinogenesis and are considered biomarkers of novel cancer and other diseases Diamandis et al. (2000). Previous studies have suggested that the major effector or peptide angiotensin II of the renin-angiotensin system can induce a cascade of pro-inflammatory responses in response to BPA treatment by increasing leukocyte-endothelial interactions, ROS production, and pro-inflammatory cytokine accumulation Zhang et al. (2020). The other modules also suggested changes in immune-related functions, similar to other WGCNA results. Hence, BPA induces abnormalities in sperm signaling and alters the immunoreactivity of the spleen and thymus. This suggests a robust response to BPA characterized by an abnormal immune response linked to carcinogenesis.

Overall, the findings of this study suggest that BPA exposure can have a profound impact on the immune system. Further research is essential to gain a deeper understanding of the mechanisms by which BPA disrupts immune function and its potential long-term health effects, to develop effective strategies to mitigate BPA-mediated toxicity.

5. Conclusion

Our comprehensive analysis of RNA-seq data from 20 different mouse tissues exposed to BPA sheds light on the extensive impact of this endocrine disruptor. Our findings highlight the significant effect of BPA exposure on various tissues, especially the thymus that emerged as the most susceptible organ, followed by the colon, liver, lung, kidney, skeletal muscle, spleen, stomach, and sperm. The identification of immune response activation pathways in most BPA-exposed tissues, particularly the elevated expression of genes related to T cell receptors, strongly suggests an orchestrated immune reaction initiated by the migration of immune cells from the thymus, where T cell maturation occurs.

Moreover, our analyses suggest metabolism suppression across different tissues, raising concerns about the development of associated diseases in the affected organ. The in-depth study of transcriptome, which includes the molecular responses of these tissues to BPA exposure, provides a valuable resource for understanding the intricate effects of endocrine disruptors on body and tissue functions. To the best of our knowledge, this is the first report decoding the response to BPA exposure in 20 tissues. This approach not only enhances our ability to discern the impacts of hazardous materials such as BPA, but also contributes to the broader exploration of biological functions in response to toxic substances.

Acknowledgements

This research was supported by the Basic Science Research Program through the National Research Foundation of Korea (NRF) funded by the Ministry of Education (NRF-2018R1A6A1A03025159).

Author contributions

Yejee Park: conceptualization, methodology, formal analysis, writing – original draft. Min-Jae Jang: methodology, writing – review and editing. Do-Yeal Ryu: data curation. Byeonghwi Lim: writing – review and editing. Rajesh Kumar Pathak: writing – review and editing. Myung-Geol Pang: conceptualization, data curation. Jun-Mo Kim: conceptualization, writing – review and editing, supervision.

Disclosure statement

No potential conflict of interest was reported by the author(s).

Funding

This work was supported by National Research Foundation of Korea: [Grant Number NRF-2018R1A6A1A03025159].

Data availability

Data will be made available upon request.

ORCID

Jun-Mo Kim  <http://orcid.org/0000-0002-6934-398X>

References

Abbassi-Daloui T, El Abdellaoui S, Voortman LM, Veeger TT, Cats D, Mei H, Meuffels DE, van Arkel E, AC't Hoen P, Kan HE, Raz

- V. 2023. A transcriptome atlas of leg muscles from healthy human volunteers reveals molecular and cellular signatures associated with muscle location. *Elife*. **12**:e80500. doi:10.7554/eLife.80500.
- Abraham A, Chakraborty P. 2020. A review on sources and health impacts of bisphenol A. *Rev Environ Health*. **35** (2):201–210. doi:10.1515/reveh-2019-0034.
- Acconcia F, Pallottini V, Marino M. 2015. Molecular mechanisms of action of BPA. *Dose Response*. **13**(4):1559325815610582. doi:10.1177/1559325815610582.
- Adegoke EO, Rahman MS, Pang M-G. 2020. Bisphenols threaten male reproductive health via testicular cells. *Front Endocrinol (Lausanne)*. **11**:624. doi:10.3389/fendo.2020.00624.
- Ahn JS, Won JH, Kim DY, Jung SE, Kim BJ, Kim JM, Ryu BY. 2022. Transcriptome alterations in spermatogonial stem cells exposed to bisphenol A. *Animal Cells Syst (Seoul)*. **26** (2):70–83. doi:10.1080/19768354.2022.2061592.
- Andrews S. 2012. FastQC: A quality control application for high throughput sequence data. *Babraham Institute Project page*: <http://www.bioinformatics.bbsrc.ac.uk/projects/fastqc>.
- Aydemir I, Kum Ş, Tuğlu Mİ. 2018. Histological investigations on thymus of male rats prenatally exposed to bisphenol A. *Chemosphere*. **206**:1–8. doi:10.1016/j.chemosphere.2018.04.145.
- Benjamini Y, Hochberg Y. 1995. Controlling the false discovery rate: a practical and powerful approach to multiple testing. *J R Stat Soc B: Stat Methodol*. **57**(1):289–300. doi:10.1111/j.2517-6161.1995.tb02031.x.
- Bolger AM, Lohse M, Usadel B. 2014. Trimmomatic: a flexible trimmer for Illumina sequence data. *Bioinformatics*. **30** (15):2114–2120. doi:10.1093/bioinformatics/btu170.
- Castellini C, Totaro M, Parisi A, D'Andrea S, Lucente L, Cordeschi G, Francavilla S, Francavilla F, Barbonetti A. 2020. Bisphenol A and male fertility: Myths and realities. *Front Endocrinol (Lausanne)*. **353**. doi:10.3389/fendo.2020.00353.
- Chen ZJ, Yang XL, Liu H, Wei W, Zhang KS, Huang HB, Giesy JP, Liu HL, Du J, Wang HS. 2015. Bisphenol A modulates colorectal cancer protein profile and promotes the metastasis via induction of epithelial to mesenchymal transitions. *Arch Toxicol*. **89**:1371–1381. doi:10.1007/s00204-014-1301-z.
- Chevalier N, Vega A, Bouskine A, Siddeek B, Michiels JF, Chevallier D, Fenichel P. 2012. GPR30, the non-classical membrane G protein related estrogen receptor, is overexpressed in human seminoma and promotes seminoma cell proliferation. *PLoS One*. **7**(4):e34672. doi:10.1371/journal.pone.0034672.
- Collins C, Norris S, McEntee G, Traynor O, Bruno L, von Boehmer H, Hegarty J, O'Farrelly C. 1996. RAG1, RAG2 and pre-T cell receptor α chain expression by adult human hepatic T cells: evidence for extrathymic T cell maturation. *Eur J Immunol*. **26**(12):3114–3118. doi:10.1002/eji.1830261243.
- Corda PO, Santiago J, Fardilha M. 2022. G-Protein Coupled Receptors in Human Sperm: An In Silico Approach to Identify Potential Modulatory Targets. *Molecules*. **27** (19):6503. doi:10.3390/molecules27196503.
- Costa HE, Cairrao E. 2024. Effect of bisphenol A on the neurological system: A review update. *Arch Toxicol*. **98**(1):1–73. doi:10.1007/s00204-023-03614-0.
- Dennis G, et al. 2003. DAVID: database for annotation, visualization, and integrated discovery. *Genome Biol*. **4**(9):R60. doi:10.1186/gb-2003-4-9-r60.

- Diamandis EP, Yousef GM, Luo LY, Magklara A, Obiezu CV. 2000. The new human kallikrein gene family: implications in carcinogenesis. *Trends Endocrinol Metab.* **11**(2):54–60. doi:10.1016/S1043-2760(99)00225-8.
- Drobná Z, Henriksen AD, Wolstenholme JT, Montiel C, Lambeth PS, Shang S, Harris EP, Zhou C, Flaws JA, Adli M, Rissman EF. 2018. Transgenerational effects of bisphenol A on gene expression and DNA methylation of imprinted genes in brain. *Endocrinology.* **159**(1):132–144. doi:10.1210/en.2017-00730.
- El-Hefnawy SM, Kasemy ZA, Eid HA, Elmadbouh I, Mostafa RG, Omar TA, Kasem HE, Ghonaim EM, Ghonaim MM, Saleh AA. 2022. Potential impact of serpin peptidase inhibitor clade (A) member 4 SERPINA4 (rs2093266) and SERPINA5 (rs1955656) genetic variants on COVID-19 induced acute kidney injury. *Human Gene.* **32**:101023. doi:10.1016/j.mgene.2022.101023.
- Fang L, Cai W, Liu S, Canela-Xandri O, Gao Y, Jiang J, Rawlik K, Li B, Schroeder SG, Rosen BD, Li CJ. 2020. Comprehensive analyses of 723 transcriptomes enhance genetic and biological interpretations for complex traits in cattle. *Genome Res.* **30**(5):790–801. doi:10.1101/gr.250704.119.
- Gao DD, Lan CF, Cao XN, Chen L, Lei TL, Peng L, Xu JW, Qiu ZE, Wang LL, Sun Q, Huang ZY. 2022. G protein-coupled estrogen receptor promotes acrosome reaction via regulation of Ca²⁺ signaling in mouse sperm. *Biol Reprod.* **107**(4):1026–1034.
- Gao Q, Yue Y, Min M, Peng S, Shi Z, Wang J, Zhang T. 2018. Time-series transcriptomic analysis of the kelp grouper *Epinephelus moara* in response to low salinity stress. *Animal Cells Syst (Seoul).* **22**(4):234–242. doi:10.1080/19768354.2018.1487335.
- Gassman NR. 2017. Induction of oxidative stress by bisphenol A and its pleiotropic effects. *Environ Mol Mutagen.* **58**(2):60–71. doi:10.1002/em.22072.
- González-Rojo S, Lombó M, Fernández-Díez C, Herráez MP. 2019. Male exposure to bisphenol a impairs spermatogenesis and triggers histone hyperacetylation in zebrafish testes. *Environ Pollut.* **248**:368–379. doi:10.1016/j.envpol.2019.01.127.
- Guarnotta V, Amodei R, Frasca F, Aversa A, Giordano C. 2022. Impact of chemical endocrine disruptors and hormone modulators on the endocrine system. *Int J Mol Sci.* **23**(10):5710. doi:10.3390/ijms23105710.
- Gurmeet KSS, Rosnah I, Normadiyah MK, Das S, Mustafa AM. 2014. Detrimental effects of bisphenol A on development and functions of the male reproductive system in experimental rats. *EXCLI J.* **13**:151.
- Ha J, Shin J, Seok E, Kim S, Sun S, Yang H. 2023. Estradiol and progesterone regulate NUCB2/nesfatin-1 expression and function in GH3 pituitary cells and THESC endometrial cells. *Animal Cells Syst (Seoul).* **27**(1):129–137. doi:10.1080/19768354.2023.2226735.
- Hackl C, Lang SA, Moser C, Mori A, Fichtner-Feigl S, Hellerbrand C, Dietmeier W, Schlitt HJ, Geissler EK, Stoeltzing O. 2010. Activating transcription factor-3 (ATF3) functions as a tumor suppressor in colon cancer and is up-regulated upon heat-shock protein 90 (Hsp90) inhibition. *BMC Cancer.* **10**:1–9. doi:10.1186/1471-2407-10-668.
- Hendriks J, Gravestien LA, Tesselaar K, Van Lier RA, Schumacher TN, Borst J. 2000. CD27 is required for generation and long-term maintenance of T cell immunity. *Nat Immunol.* **1**(5):433–440. doi:10.1038/80877.
- Hengstler JG, Foth H, Gebel T, Kramer PJ, Lilienblum W, Schweinfurth H, Völkel W, Wollin KM, Gundert-Remy U. 2011. Critical evaluation of key evidence on the human health hazards of exposure to bisphenol A. *Crit Rev Toxicol.* **41**(4):263–291. doi:10.3109/10408444.2011.558487.
- Hu C, Yang J, Qi Z, Wu H, Wang B, Zou F, Mei H, Liu J, Wang W, Liu Q. 2022. Heat shock proteins: Biological functions, pathological roles, and therapeutic opportunities. *MedComm.* **3**(3):e161. doi:10.1002/mco2.161.
- Hwang KA, Park SH, Yi BR, Choi KC. 2011. Gene alterations of ovarian cancer cells expressing estrogen receptors by estrogen and bisphenol a using microarray analysis. *Lab Anim Res.* **27**(2):99–107. doi:10.5625/lar.2011.27.2.99.
- Jalal N, Surendranath AR, Pathak JL, Yu S, Chung CY. 2018. Bisphenol A (BPA) the mighty and the mutagenic. *Toxicol Rep.* **5**:76–84. doi:10.1016/j.toxrep.2017.12.013.
- Jung J, Mok C, Lee W, Jang W. 2017. Meta-analysis of microarray and RNA-Seq gene expression datasets for carcinogenic risk: An assessment of Bisphenol A. *Mol Cell Toxicol.* **13**(2):239–249. doi:10.1007/s13273-017-0026-5.
- Kabir ER, Rahman MS, Rahman I. 2015. A review on endocrine disruptors and their possible impacts on human health. *Environ Toxicol Pharmacol.* **40**(1):241–258. doi:10.1016/j.etap.2015.06.009.
- Kelly M, Connolly L, Dean M. 2020. Public awareness and risk perceptions of endocrine disrupting chemicals: a qualitative study. *Int J Environ Res Public Health.* **17**(21):7778. doi:10.3390/ijerph17217778.
- Kim CH, Kim MJ, Park J, Kim J, Kim JY, An MJ, Shin GS, Lee HM, Kim JW. 2021. Bisphenol A exposure changes the transcriptomic and proteomic dynamics of human retinoblastoma Y79 Cells. *Genes (Basel).* **12**(2):264. doi:10.3390/genes12020264.
- Kim D, Paggi JM, Park C, Bennett C, Salzberg SL. 2019. Graph-based genome alignment and genotyping with HISAT2 and HISAT-genotype. *Nat Biotechnol.* **37**(8):907–915. doi:10.1038/s41587-019-0201-4.
- Kourouma A, Quan C, Duan P, Qi S, Yu T, Wang Y, Yang K. 2015. Bisphenol A induces apoptosis in liver cells through induction of ROS. *Adv Toxicol.* **2015**:1–10.
- Krzastek SC, Farhi J, Gray M, Smith RP. 2020. Impact of environmental toxin exposure on male fertility potential. *Transl Androl Urol.* **9**(6):2797. doi:10.21037/tau-20-685.
- Kukurba KR, Montgomery SB. 2015. RNA sequencing and analysis. *Cold Spring Harb Protoc.* **2015**(11):951. doi:10.1101/pdb.top084970.
- La Merrill MA, Vandenberg LN, Smith MT, Goodson W, Browne P, Patisaul HB, Guyton KZ, Kortenkamp A, Coglianò VJ, Woodruff TJ, Rieswijk L. 2020. Consensus on the key characteristics of endocrine-disrupting chemicals as a basis for hazard identification. *Nat Rev Endocrinol.* **16**(1):45–57. doi:10.1038/s41574-019-0273-8.
- Lang BJ, Guerrero ME, Prince TL, Okusha Y, Bonorino C, Calderwood SK. 2021. The functions and regulation of heat shock proteins; key orchestrators of proteostasis and the heat shock response. *Arch Toxicol.* **95**(6):1943–1970. doi:10.1007/s00204-021-03070-8.
- Langfelder P, Horvath S. 2008. WGCNA: an R package for weighted correlation network analysis. *BMC Bioinf.* **9**(1):1–13. doi:10.1186/1471-2105-9-559.
- Lee HS, Park Y. 2019. Identification of metabolic pathways related to the bisphenol A-induced adipogenesis in

- differentiated murine adipocytes by using RNA-sequencing. *Environ Res.* **171**:161–169. doi:10.1016/j.envres.2019.01.017.
- Li H, Handsaker B, Wysoker A, Fennell T, Ruan J, Homer N, Marth G, Abecasis G, Durbin R. 2009. The sequence alignment/map format and SAMtools. *Bioinformatics.* **25** (16):2078–2079. doi:10.1093/bioinformatics/btp352.
- Liao Y, Smyth GK, Shi W. 2014. featureCounts: an efficient general purpose program for assigning sequence reads to genomic features. *Bioinformatics.* **30**(7):923–930. doi:10.1093/bioinformatics/btt656.
- Ma Y, Liu H, Wu J, Yuan L, Wang Y, Du X, Wang R, Marwa PW, Petlulu P, Chen X, Zhang H. 2019. The adverse health effects of bisphenol A and related toxicity mechanisms. *Environ Res.* **176**:108575. doi:10.1016/j.envres.2019.108575.
- Manzoor MF, Tariq T, Fatima B, Sahar A, Tariq F, Munir S, Khan S, Nawaz Ranjha MMA, Sameen A, Zeng XA, Ibrahim SA. 2022. An insight into bisphenol A, food exposure and its adverse effects on health: A review. *Front Nutr.* **9**:1047827. doi:10.3389/fnut.2022.1047827.
- Massari S, Bellini M, Ciccarese S, Antonacci R. 2018. Overview of the germline and expressed repertoires of the TRB genes in *Sus scrofa*. *Front Immunol.* **9**:2526. doi:10.3389/fimmu.2018.02526.
- Matuszczak E, Komarowska MD, Debek W, Hermanowicz A. 2019. The impact of bisphenol A on fertility, reproductive system, and development: a review of the literature. *Int J Endocrinol.* **2019**. doi:10.1155/2019/4068717.
- Melzer D, Osborne NJ, Henley WE, Cipelli R, Young A, Money C, McCormack P, Luben R, Khaw KT, Wareham NJ, Galloway TS. 2012. Urinary bisphenol A concentration and risk of future coronary artery disease in apparently healthy men and women. *Circulation.* **125**(12):1482–1490. doi:10.1161/CIRCULATIONAHA.111.069153.
- Murata M, Kang J-H. 2018. Bisphenol A (BPA) and cell signaling pathways. *Biotechnol Adv.* **36**(1):311–327. doi:10.1016/j.biotechadv.2017.12.002.
- Mure LS, Le HD, Benegiamo G, Chang MW, Rios L, Jillani N, Ngotho M, Kariuki T, Dkhissi-Benyahya O, Cooper HM, Panda S. 2018. Diurnal transcriptome atlas of a primate across major neural and peripheral tissues. *Science.* **359** (6381):eaao0318.
- Niemira M, Collin F, Szalkowska A, Bielska A, Chwialkowska K, Reszec J, Niklinski J, Kwasniewski M, Kretowski A. 2019. Molecular signature of subtypes of non-small-cell lung cancer by large-scale transcriptional profiling: identification of key modules and genes by weighted gene co-expression network analysis (WGCNA). *Cancers (Basel).* **12**(1):37. doi:10.3390/cancers12010037.
- Norreen-Thorsen M, Struck EC, Öling S, Zwahlen M, Von Feilitzen K, Odeberg J, Lindskog C, Ponten F, Uhlen M, Dusart PJ, Butler LM. 2022. A human adipose tissue cell-type transcriptome atlas. *Cell Rep.* **40**(2). doi:10.1016/j.celrep.2022.111046.
- Papaconstantinou AD, Fisher BR, Umbreit TH, Goering PL, Lappas NT, Brown KM. 2001. Effects of β -estradiol and bisphenol A on heat shock protein levels and localization in the mouse uterus are antagonized by the antiestrogen ICI 182,780. *Toxicol Sci.* **63**(2):173–180. doi:10.1093/toxsci/63.2.173.
- Park D, Yu Y, Kim JH, Lee J, Park J, Hong K, Seo JK, Lim C, Min KT. 2023. Suboptimal Mitochondrial Activity Facilitates Nuclear Heat Shock Responses for Proteostasis and Genome Stability. *Mol Cells.* **46**(6):374–386. doi:10.14348/molcells.2023.2181.
- Pertea M, Pertea GM, Antonescu CM, Chang TC, Mendell JT, Salzberg SL. 2015. StringTie enables improved reconstruction of a transcriptome from RNA-seq reads. *Nat Biotechnol.* **33**(3):290–295. doi:10.1038/nbt.3122.
- Pilot Program Disrupts Endocrine Disrupting Chemicals. 2023-08-29; Available from: <https://campuslifeservices.home.ucsf.edu/sustainability/news/pilot-program-disrupts-endocrine-disrupting-chemicals>.
- Radwan M, Wielgomas B, Dziejirska E, Radwan P, Kałużny P, Klimowska A, Hanke W, Jurewicz J. 2018. Urinary bisphenol A levels and male fertility. *Am J Mens Health.* **12**(6):2144–2151. doi:10.1177/1557988318799163.
- Rahman MS, Pang M-G. 2019. Understanding the molecular mechanisms of bisphenol A action in spermatozoa. *Clin Exp Reprod Med.* **46**(3):99. doi:10.5653/cerm.2019.00276.
- Ren X, Li T, Zhang W, Yang X. 2022. Targeting heat-shock protein 90 in cancer: an update on combination therapy. *Cells.* **11**(16):2556. doi:10.3390/cells11162556.
- Ritchie ME, Phipson B, Wu DI, Hu Y, Law CW, Shi W, Smyth GK. 2015. Limma powers differential expression analyses for RNA-sequencing and microarray studies. *Nucleic Acids Res.* **43**(7):e47–e47. doi:10.1093/nar/gkv007.
- Robinson MD, McCarthy DJ, Smyth GK. 2010. edgeR: a Bioconductor package for differential expression analysis of digital gene expression data. *Bioinformatics.* **26**(1):139–140. doi:10.1093/bioinformatics/btp616.
- Robinson MD, Oshlack A. 2010. A scaling normalization method for differential expression analysis of RNA-seq data. *Genome Biol.* **11**(3):1–9. doi:10.1186/gb-2010-11-3-r25.
- Rochester JR. 2013. Bisphenol A and human health: a review of the literature. *Reprod Toxicol.* **42**:132–155. doi:10.1016/j.reprotox.2013.08.008.
- Sadek KM, Abouzed TK, Ayoub MA. 2014. Oxidative and hormonal disruptions underlie bisphenol a-induced testicular toxicity in male rabbits. *J Bioeng Life Sci.* **8** (11):1174–1180.
- Sánchez-Navarro A, González-Soria I, Caldiño-Bohn R, Bobadilla NA. 2021. An integrative view of serpins in health and disease: the contribution of SerpinA3. *Am J Physiol-Cell Physiol.* **320**(1):C106–C118.
- Satam H, Joshi K, Mangrolia U, Waghoo S, Zaidi G, Rawool S, Thakare RP, Banday S, Mishra AK, Das G, Malonia SK. 2023. Next-generation sequencing technology: Current trends and advancements. *Biology (Basel).* **12**(7):997. doi:10.3390/biology12070997.
- Struyf A, Hubert M, Rousseeuw P. 1997. Clustering in an object-oriented environment. *J Stat Softw.* **1**:1–30.
- Sukjamnong S, Thongkorn S, Kanlayaprasit S, Saeliw T, Hussem K, Warayanon W, Hu VW, Tencomnao T, Sarachana T. 2020. Prenatal exposure to bisphenol A alters the transcriptome-interactome profiles of genes associated with Alzheimer's disease in the offspring hippocampus. *Sci Rep.* **10**(1):9487. doi:10.1038/s41598-020-65229-0.
- Supek F, Bošnjak M, Škunca N, Šmuc T. 2011. REVIGO summarizes and visualizes long lists of gene ontology terms. *PLoS One.* **6**(7):e21800. doi:10.1371/journal.pone.0021800.
- Tyl RW. 2009. Basic exploratory research versus guideline-compliant studies used for hazard evaluation and risk assessment: bisphenol A as a case study. *Environ Health Perspect.* **117**(11):1644–1651. doi:10.1289/ehp.0900893.

- Vom Saal FS, Nagel SC, Coe BL, Angle BM, Taylor JA. 2012. The estrogenic endocrine disrupting chemical bisphenol A (BPA) and obesity. *Mol Cell Endocrinol.* **354**(1-2):74–84. doi:10.1016/j.mce.2012.01.001.
- Vom Saal FS, Vandenberg LN. 2021. Update on the health effects of bisphenol A: overwhelming evidence of harm. *Endocrinology.* **162**(3):bqaa171. doi:10.1210/endo/bqaa171.
- Wan Y, Kertesz M, Spitale RC, Segal E, Chang HY. 2011. Understanding the transcriptome through RNA structure. *Nat Rev Genet.* **12**(9):641–655. doi:10.1038/nrg3049.
- Wang D, Eraslan B, Wieland T, Hallström B, Hopf T, Zolg DP, Zecha J, Asplund A, Li LH, Meng C, Frejino M. 2019. A deep proteome and transcriptome abundance atlas of 29 healthy human tissues. *Mol Syst Biol.* **15**(2):e8503. doi:10.15252/msb.20188503.
- Watson-Haigh NS, Kadarmideen HN, Reverter A. 2010. PCIT: an R package for weighted gene co-expression networks based on partial correlation and information theory approaches. *Bioinformatics.* **26**(3):411–413. doi:10.1093/bioinformatics/btp674.
- Weis WI, Kobilka BK. 2018. The molecular basis of G protein-coupled receptor activation. *Annu Rev Biochem.* **87**:897–919. doi:10.1146/annurev-biochem-060614-033910.
- Wickham H. 2011. *Wiley Interdiscip. Rev. Comput Stat.* **3**(2):180–185.
- Wisniewski P, Romano RM, Kizys MM, Oliveira KC, Kasamatsu T, Giannocco G, Chiamolera MI, Dias-da-Silva MR, Romano MA. 2015. Adult exposure to bisphenol A (BPA) in Wistar rats reduces sperm quality with disruption of the hypothalamic–pituitary–testicular axis. *Toxicology.* **329**:1–9. doi:10.1016/j.tox.2015.01.002.
- Xi W, Lee CKF, Yeung WSB, Giesy JP, Wong MH, Zhang X, Hecker M, Wong CK. 2011. Effect of perinatal and postnatal bisphenol A exposure to the regulatory circuits at the hypothalamus–pituitary–gonadal axis of CD-1 mice. *Reprod Toxicol.* **31**(4):409–417. doi:10.1016/j.reprotox.2010.12.002.
- Xu ZS, Li ZY, Chen Y, Chen M, Li LC, Ma YZ. 2012. Heat shock protein 90 in plants: molecular mechanisms and roles in stress responses. *Int J Mol Sci.* **13**(12):15706–15723. doi:10.3390/ijms131215706.
- Yin R, Gu L, Li M, Jiang C, Cao T, Zhang X. 2014. Gene expression profiling analysis of bisphenol A-induced perturbation in biological processes in ER-negative HEK293 cells. *PLoS One.* **9**(6):e98635. doi:10.1371/journal.pone.0098635.
- Yoshino S, Yamaki K, Li X, Sai T, Yanagisawa R, Takano H, Taneda S, Hayashi H, Mori Y. 2004. Prenatal exposure to bisphenol A up-regulates immune responses, including T helper 1 and T helper 2 responses, in mice. *Immunology.* **112**(3):489–495. doi:10.1111/j.1365-2567.2004.01900.x.
- Zhang B, Horvath S. 2005. A general framework for weighted gene co-expression network analysis. *Stat Appl Genet Mol Biol.* **4**(1). doi:10.2202/1544-6115.1128.
- Zhang Y, Shi Y, Li Z, Sun L, Zhang M, Yu L, Wu S. 2020. BPA disrupts 17-estradiol-mediated hepatic protection against ischemia/reperfusion injury in rat liver by upregulating the Ang II/AT1R signaling pathway. *Mol Med Rep.* **22**(1):416–422.
- Zheng G, Huang T. 2018. The reconstruction and analysis of gene regulatory networks. *Comput Syst Biol: Methods Protoc.* 1754:137–154.